Chinese Journal of
POLYMER SCIENCE

RESEARCH ARTICLE

https://doi.org/10.1007/s10118-026-3668-8
Chinese J. Polym. Sci. **2026**, *44*, 2748–2757

Regulation of Microphase Separation in Bio-based Thermoplastic Polyurethanes Driven by Hard Segment Content

De-Xian Yin†, Yu-Qiong Hu†, Ya-Nan Cheng, Shuo Yan, Zi-Lin Liu, Yi-Qing Wang*, Shi-Kai Hu*, and Xiu-Ying Zhao*

State Key Laboratory of Organic-Inorganic Composites, Beijing University of Chemical Technology, Beijing 100029, China

Electronic Supplementary Information

Abstract Regulation of the microphase-separated structure is critical for high-performance thermoplastic polyurethanes (TPUs). To address the limitations of poor heat resistance and reliance on petrochemical resources in traditional TPUs, bio-based TPUs were engineered using rigid 1,4-phenylene diisocyanate and bio-based poly(trimethylene ether) glycol. The results demonstrate that microstructural evolution, hydrogen bonding network formation, and tailoring of macroscopic properties in TPUs can be realized by varying the hard segment content. Increasing the hard segment content enhanced microstructural ordering, boosting the tensile strength from 6.1 MPa to 22.6 MPa while maintaining an elongation at break above 600%. Crucially, the robust crystalline network enhanced thermal stability of the TPUs, resulting in a maximum 5% thermal deformation temperature of 230.2 °C for TPUs. This work elucidates the structure-property relationships governing microphase separation, empowering the rational design of bio-based materials with exceptional toughness and thermal resistance.

Keywords Thermoplastic polyurethane; 1,4-Phenylene diisocyanate; Bio-based poly(trimethylene ether) glycol; Microphase separation; Hydrogen bonding

Citation: Yin, D. X.; Hu, Y. Q.; Cheng, Y. N.; Yan, S.; Liu, Z. L.; Wang, Y. Q.; Hu, S. K.; Zhao, X. Y. Regulation of microphase separation in bio-based thermoplastic polyurethanes driven by hard segment content. *Chinese J. Polym. Sci.* **2026**, *44*, 2748–2757.

INTRODUCTION

Thermoplastic polyurethanes (TPUs) are linear block copolymers consisting of alternating flexible polyol soft segments and rigid hard segments composed of isocyanates and chain extenders.[1,2] Combining the high elasticity of vulcanized rubber with the melt processability of thermoplastics, TPUs can be efficiently formed *via* injection molding and extrusion, leading to their widespread application in the automotive, medical, electronic, and sports equipment fields.[3] Microstructurally, the soft segments endow the material with flexibility and low-temperature elasticity, whereas the hard segments aggregate driven by strong intermolecular hydrogen bonding to form hard domains that act as physical crosslinks, providing mechanical strength and thermal stability.[4,5] Based on this unique two-phase microstructure, the properties of TPUs can be precisely tailored by regulating the chemical composition, ratio, and molecular weight of the soft and hard segments.[6]

The macroscopic properties of TPUs are intrinsically governed by their microscopic microphase separation structure.[7–12] Prior research emphasizes that promoting phase separation and establishing well-defined, uniform hard domains is pivotal for reconciling high strength with superior elasticity in TPUs.[13–16] For instance, recent studies have demonstrated that introducing fluorine-hydrogen bonds can induce a self-confined effect, driving the *in situ* formation of ultra-small and dense hard nanodomains. This tailored microphase separation structure successfully achieved simultaneous enhancement of mechanical robustness, self-healing, and ionic conductivity in elastomers.[17,18] Among the various isocyanates, 1,4-phenylene diisocyanate (PPDI) possesses a distinct rigid planar benzene skeleton and high molecular symmetry.[19] This unique architecture facilitates the dense packing of hard segments through intense intermolecular hydrogen bonding, which promotes robust crystallization. Consequently, the resulting microdomain rigidity and thermal stability of PPDI surpass those of conventional isocyanates such as toluene diisocyanate and methylene diphenyl diisocyanate. Owing to its superior structural symmetry, PPDI is an ideal candidate for effectively modulating microphase separation behavior to engineer high-performance TPUs.[20]

Notably, the heavy reliance of conventional commercial TPUs on non-renewable petrochemical resources has exacerbated resource depletion and environmental burdens, cat-

* Corresponding authors, E-mail: wangyq1@mail.buct.edu.cn (Y.Q.W.)
E-mail: skhu@mail.buct.edu.cn (S.K.H.)
E-mail: zhaoxy@mail.buct.edu.cn (X.Y.Z.)
† These authors contributed equally to this work.
Received January 30, 2026; Accepted March 15, 2026; Published online June 3, 2026

alyzing a strategic transition in both academia and industry toward sustainable, bio-based alternatives. Bio-based poly(trimethylene ether) glycol (PO3G), derived from bio-based 1,3-propanediol or glycerol, is an emerging soft segment with a significantly lower carbon footprint, aligning well with the urgent demand for sustainable polymeric materials.[21] From a molecular perspective, the critical feature of PO3G is its repeating unit containing three methylene groups. Owing to the odd-even effect, this odd-numbered carbon structure induces polymer chains to adopt an asymmetric twisted conformation. This conformation significantly hinders regular chain packing and crystallization, maintaining a highly amorphous state at room temperature. This low-crystallinity soft segment not only endows the TPU with excellent elastic recovery and low hysteresis, but also provides a flexible environment for the independent crystallization of hard segments, thereby thermodynamically driving the refinement of the microphase-separated structure.[22]

In this study, a series of bio-based TPU elastomers with systematically graded hard segment content were prepared by molecularly designing bio-based PO3G soft segments with highly symmetrical PPDI and 1,4-butanediol (BDO) hard segments. Utilizing thermal analysis, mechanical testing, dynamic mechanical analysis, and micro-morphological characterization, this study aims to systematically reveal the intrinsic driving mechanism of hard segment content on microphase separation behavior and to analyze the regulation laws governing the evolution of the aggregation structure and crystallization behavior. In addition to verifying the potential of bio-based materials in high-performance applications, this study also provides critical theoretical guidance and structural regulation strategies for the design of novel TPUs with high mechanical strength, superior heat resistance, and environmental friendliness.

EXPERIMENTAL

Materials

PPDI (purity ≥98%) was purchased from Zhejiang Lishui Youbang New Material Co., Ltd. (Lishui, China). BDO (purity ≥ 99.7%) was obtained from Shanghai Macklin Biochemical Co., Ltd. (Shanghai, China). Bio-based PO3G (M_n=1000 g/mol) was supplied by Guangzhou Haoyi New Material Technology Co., Ltd. (Guangzhou, China). All the chemicals were used as received without further purification.

Synthesis and Sample Preparation

The bio-based TPUs were synthesized using a two-step prepolymer method. Compared to one-shot random polymerization, this specific stepwise feeding sequence was strategically employed to precisely regulate the sequence structure of the polymer chains, ensuring the formation of well-defined alternating soft and hard blocks. As highlighted in recent studies, such precise sequence control serves as a thermodynamic foundation for driving robust microphase separation and enhancing macroscopic properties.[23] First, the bio-based polyol PO3G was degassed at 110 °C under vacuum (<0.095 MPa) for 1.5 h to remove moisture. After cooling to 75 °C, the calculated amount of PPDI was added under a dry nitrogen atmosphere. The mixture was mechanically stirred at 300 r/min for 1.5 h to obtain an isocyanate-terminated prepolymer. Subsequently, chain extender BDO was added, followed by rapid stirring for 10 min to facilitate chain extension. The reaction mixture was then poured into a Teflon mold and post-cured in an air-circulating oven at 90 °C for 24 h to ensure complete reaction. The final specimens were prepared *via* compression molding: the cured TPU was preheated at 190 °C for 3 min, hot-pressed at 15 MPa for 5 min, and then cold-pressed before demolding. The specific synthesis route is shown in Fig. S1 (in the electronic supplementary information, ESI). Table S1 (in ESI) lists the detailed formulations. Corresponding to the increasing hard segment content, the samples were designated TPU18, TPU22, TPU26, TPU29, and TPU32.

Characterizations

Nuclear magnetic resonance (^{1}H-NMR)

^{1}H-NMR spectra were recorded on a Bruker AVANCE 600 MHz spectrometer using deuterated dimethyl sulfoxide as the solvent.

Gel permeation chromatography (GPC)

The number-average molecular weight and polydispersity index were determined using a Shimadzu LC-20AT system. *N*,*N*-Dimethylacetamide was used as the eluent at a flow rate of 1.0 mL/min. The results were calibrated against polystyrene standards.

Fourier transform infrared (FTIR) spectroscopy

FTIR spectra were obtained using a Bruker Tensor 27 spectrometer in the wavenumber range of 4000–600 cm^{-1} with a resolution of 4 cm^{-1} and 32 scans.

X-ray diffraction (XRD)

XRD patterns were recorded on a Rigaku D/max 2500 diffractometer with Cu Kα radiation at room temperature. The scanning range (2θ) was 5°–90° at a scanning rate of 5 (°)/min.

Small-angle X-ray scattering (SAXS)

SAXS measurements were performed using a Xenocs system equipped with a GenixCuKα source and DectrisMarCCD 345 detector. The sample-to-detector distance was set to 1300 mm, with an exposure time of 600 s.

Atom force microscope (AFM)

The phase morphology of the samples was observed using AFM (Bruker multimode8, Germany) under a quantitative nanomechanical mapping mode with a scanning frequency of 0.9 Hz.

Thermomechanical analysis (TMA)

The TMA was conducted on a TA Instruments Q400 analyzer using a cylindrical probe under a constant force of 1 N. The samples were heated from room temperature to 260 °C at a rate of 5 °C/min.

Dynamic mechanical analysis (DMA)

DMA was performed using a Mettler Toledo DMA 1 instrument in the tension mode. Rectangular specimens (30 mm × 4 mm × 1 mm) were tested at a frequency of 10 Hz and dynamic strain of 0.1%. The temperature was ramped from –100 °C to 100 °C at a rate of 3 °C/min.

Mechanical properties

Tensile tests were performed on a Zwick/Roell universal testing machine at a crosshead speed of 500 mm/min. Dumbbell-shaped specimens (30 mm × 4 mm × 1 mm) were used, and at least five specimens were tested for each sample.

https://doi.org/10.1007/s10118-026-3668-8

Thermogravimetric analysis (TGA)

Thermogravimetric analysis (TGA) was performed using a Mettler Toledo TGA/DSC 3+ system. Samples (about 5 mg) were heated from 100 °C to 600 °C at a rate of 10 °C/min under a nitrogen atmosphere.

RESULTS AND DISCUSSION

Structural Characterization

The molecular weights and distributions of the synthesized TPUs were analyzed using GPC. As shown in Fig. 1(a), all the samples exhibited sharp and symmetrical unimodal elution curves, indicating the absence of bimodal distributions or shoulder peaks. The number-average molecular weight M_n of all samples exceeded 6.6×10^4 g/mol, with the polydispersity index ($Đ$) maintained within a narrow range of 1.44–2.06. These results not only confirm the high molecular weight of the materials, but also suggest that side reactions were effectively suppressed, resulting in linear polymers with a uniform distribution.

FTIR spectroscopy was employed to confirm the formation of the chemical structure (Figs. 1b–1d).[24] The complete disappearance of the characteristic isocyanate (—NCO) band at 2275 cm^{-1}, accompanied by the emergence of N—H stretching vibrations around 3320 cm^{-1} and distinct C=O stretching vibrations in the range of 1660–1770 cm^{-1}, conclusively proves the exhaustion of the —NCO groups and successful formation of urethane bonds. Furthermore, the characteristic peaks for each component were clearly identifiable, and the benzene skeleton stretching at 1600 cm^{-1} and out-of-plane bending at 900–800 cm^{-1} confirmed the incorporation of PPDI hard segments, while the ether linkage (C—O—C) stretching at 1100 cm^{-1} was attributed to the PO3G soft segments. Notably, the absence of peaks characteristic of crosslinking byproducts, such as allophanates or biurets, further substantiates the linear, noncrosslinked structure of the synthesized TPUs.[25]

The chemical composition was further verified using ^{1}H-NMR spectroscopy (Fig. S2 in ESI). The aromatic protons of the PPDI hard segments appear at 7.3–7.4 ppm. The methylene protons adjacent to oxygen atoms (O—CH_2—) exhibit signals at 3.4 and 4.1 ppm, corresponding to PO3G and BDO units, respectively. The central methylene protons of PO3G resonate at 1.8 ppm, while those of BDO appear at 1.7 and 1.4 ppm.[26] These distinct signals confirmed that both the soft and hard segments were successfully incorporated into the polymer chain. Moreover, the actual hard segment content, calculated from the integrated peak areas using Eq. S(1) (in ESI), is consistent with the theoretical feed values, demonstrating precise control over the TPU composition during synthesis.

Analysis of the Evolution of Hydrogen Bond Interactions

Hydrogen bonding interactions act as the primary driving force for the physical crosslinking network in polyurethanes, profoundly influencing the microphase separation behavior and macroscopic properties. In the FTIR spectra, the carbonyl (C=O) stretching frequency was highly sensitive to the local microenvironment. The signal for free carbonyls was predominantly

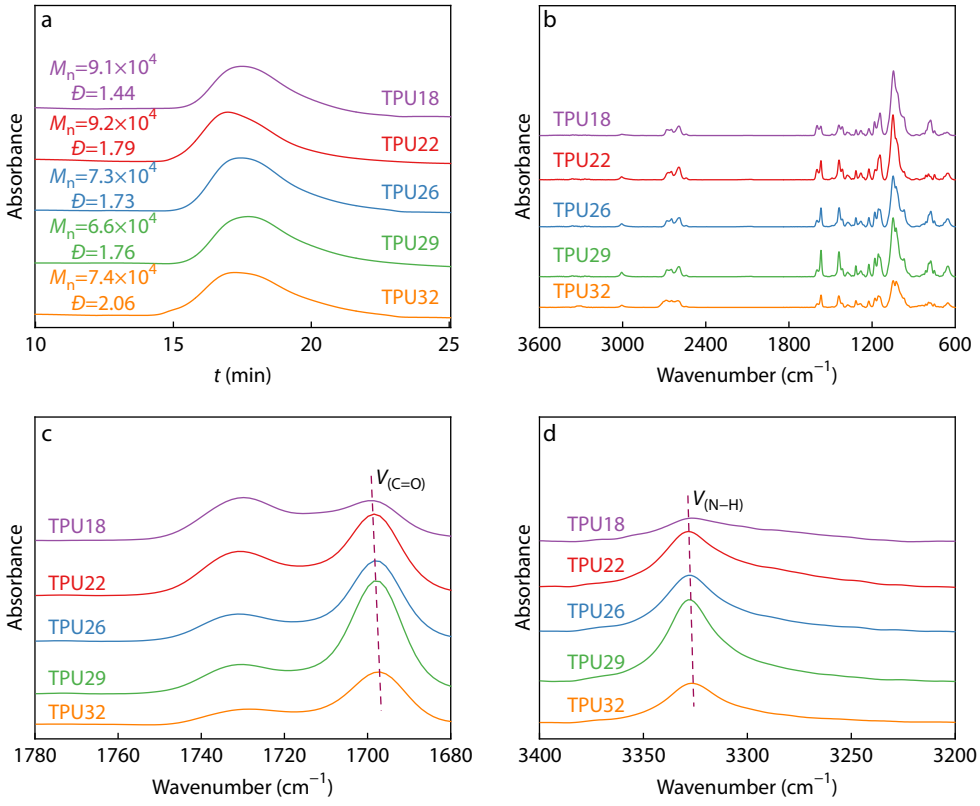

Fig. 1 (a) GPC curves of TPUs; (b) FTIR spectra (3600–600 cm^{-1}) of TPUs; (c) FTIR spectra (1780–1680 cm^{-1}) of TPUs; (d) FTIR spectra (3400–3200 cm^{-1}) of TPUs.

centered at approximately 1730 cm^{-1}. In contrast, carbonyls within the ordered hard microdomains are integrated into a robust hydrogen-bonding network; this strong interaction diminishes the C=O bond order, driving a characteristic red-shift of the stretching vibration to 1700 cm^{-1}.

Fig. 2 presents the curve-fitting results and quantitative analysis of the carbonyl region (1660–1760 cm^{-1}). As shown in Figs. 2(a)–2(e), the broad carbonyl peaks were resolved into three peaks using Gaussian functions: ordered hydrogen-bonded carbonyls (about 1700 cm^{-1}), disordered hydrogen-bonded carbonyls (about 1716 cm^{-1}), and free carbonyls (about 1730 cm^{-1}).[27–33] The high consistency between the fitted curves and the original spectra validates the reliability of this deconvolution model. The quantitative statistics (Fig. 2f and Table S2 in ESI) revealed a distinct dependence of the hydrogen bonding assembly on the hard segment content. As the hard segment content increased, the fraction of hydrogen-bonded carbonyls increased monotonically from 59.1% to 85.8%, accompanied by a corresponding decrease in the free carbonyl intensity. First, a higher hard segment content provides a greater population of donor (N—H) and acceptor (C=O) sites. Second, the rigid planar benzene skeleton and high polarity of the PPDI molecules endowed the hard segments with a high cohesive energy density. With increasing hard segment content, these strong intermolecular forces drive the hard segments to overcome steric hindrance and pack into long-range ordered structures *via* hydrogen-bonding bridges.[34] These highly ordered hard domains not only establish a robust physical crosslinking network but also exacerbate the thermodynamic incompatibility between the soft and hard segments, thereby effectively driving the refinement of microphase separation.

Evolution of Microphase-separated Structure

SAXS was employed to quantify the long period (L) of the microphase-separated structure in the reciprocal space. According to Bragg's law, domain spacing L is inversely proportional to scattering vector q ($L=2\pi/q$). As shown in the 2D SAXS patterns (Figs. 3a–3e), all the samples exhibited isotropic scattering rings, indicating the formation of periodic microphase-separated structures. The 1D integrated profiles (Fig. 3f) clearly show that the scattering peak position (q_{max}) shifted toward a lower angle (smaller q value) as the hard segment content increased. Consequently, the calculated long period L increases from 14.2 nm to 15.2 nm (detailed in Table S3 in ESI). This significant expansion is attributed to the dual effects of the hard segment volume fraction and thermodynamic driving forces. A higher hard segment content increases the volume fraction of the hard domains and exacerbates the thermodynamic incompatibility between the soft and hard segments, thereby deepening the degree of phase separation. Furthermore, highly symmetrical PPDI hard segments, driven by strong hydrogen bonding, tend to form larger and more ordered domains. The coarsening and growth of these ordered domains further increases the domain spacing.[35] To provide direct evidence in real space, AFM was used to visualize the surface morphology and provide direct evidence in real space. The 2D modulus images (Figs. 3a–3e, bottom) clearly distinguish the phase distribution, where bright, elevated regions correspond to high-modulus hard domains, and dark regions represent the low-modulus soft matrix. As the hard segment content increases, the phase contrast becomes increasingly distinct, as evidenced by the significant widening of the LogDMTModulus scale range in Figs. 3(a)–3(e).[36] The hard domains not only grow in size but also become more densely packed and interconnected, suggesting a clear morphological

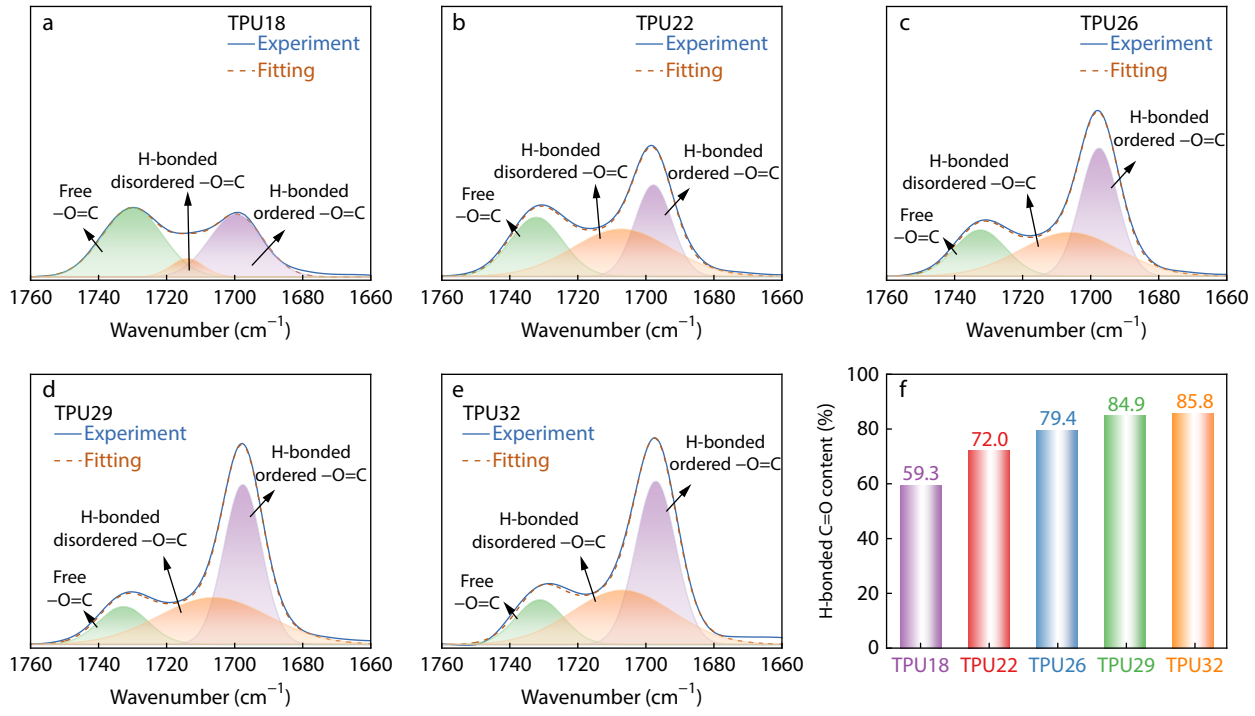

Fig. 2 (a–e) Deconvoluted C=O stretching vibration spectra of TPUs: (a) TPU18, (b) TPU22, (c) TPU26, (d) TPU29, (e) TPU32; (f) Distribution of hydrogen-bonded carbonyls as a function of hard segment content.

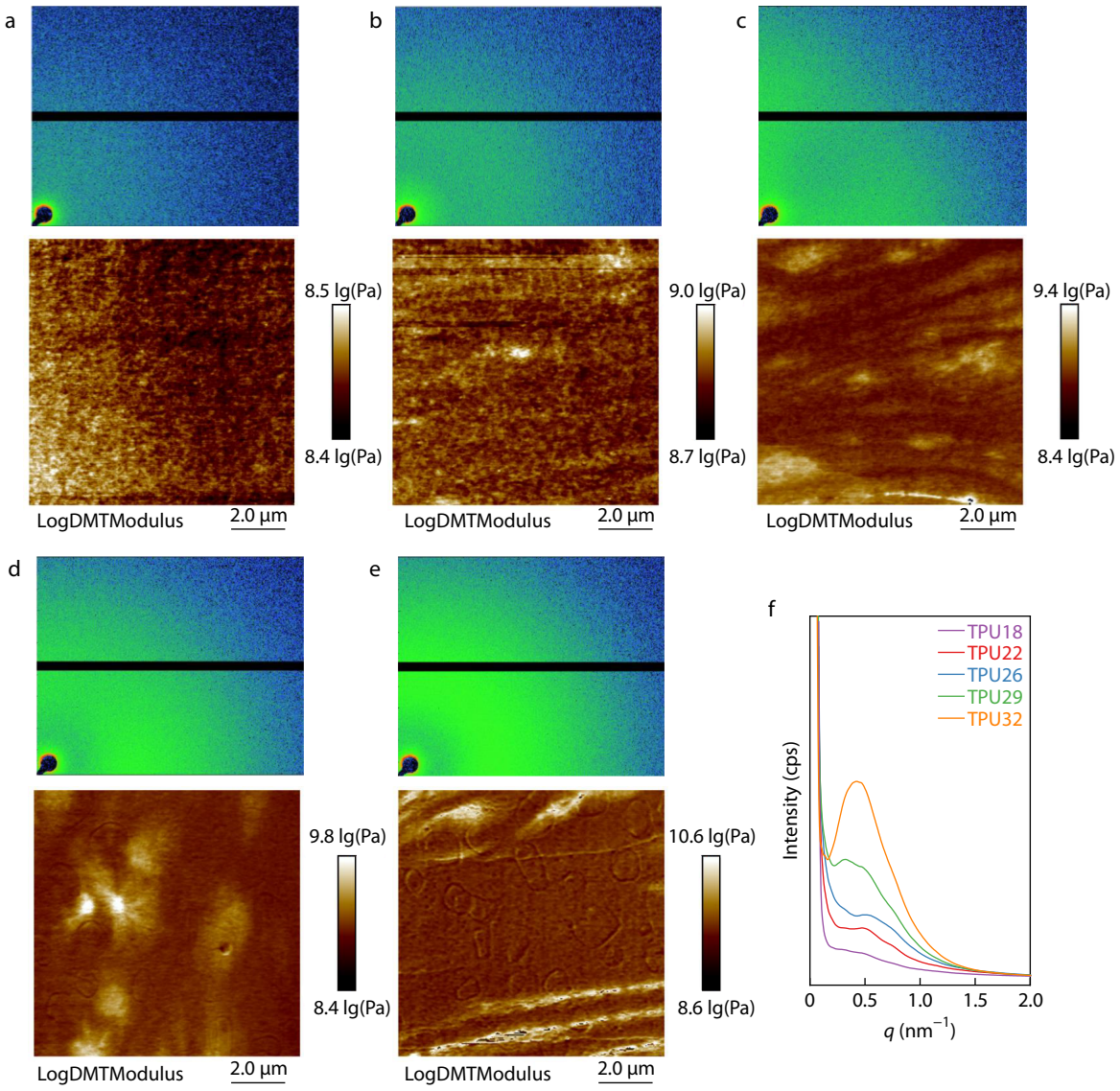

Fig. 3 (a–e) 2D SAXS patterns (top) and AFM modulus images (bottom) of TPUs; (f) 1D SAXS profiles of TPUs.

transition from a weakly phase-separated sea island to a highly robust bicontinuous structure. Statistical analysis of the 2D AFM images in Fig. S3 (in ESI) further confirms this trend, showing that the average diameter of the hard domains increased significantly from 0.027 μm in TPU18 to 0.639 μm in TPU29, while TPU32 is excluded from this quantification because its domains have completely merged into an extensively interconnected continuous network that precludes the measurement of individual sizes. These observations align perfectly with the SAXS results, confirming that increasing the PPDI hard segment content promotes the formation of a more robust and well-defined microphase-separated structure.

Fig. 4(a) illustrates the evolution of the XRD patterns with varying hard segment content. TPU18 exhibited a relatively smooth and broad diffraction peak without any distinct characteristic crystalline peaks. With increasing hard segment content, the intensity of the crystallization peaks near 19° and 24° gradually increased. These peaks corresponded to the ordered lattice packing of the PPDI hard segments, signifying their segregation from the disordered phase to form regular crystal structures. Quantitative analysis (Fig. 4b) revealed that the degree of crystallinity increased from 0.7% to 5.7% as the hard segment content increased from 18% to 32%. This enhancement was primarily attributed to an increase in the average hard segment sequence length. A higher hard segment content results in longer and more regular hard segment sequences. Driven by strong hydrogen bonding and *π*-*π* resonance in the PPDI hard segment region, these long-chain sequences can effectively overcome entropic losses caused by chain folding, resulting in dense physical crosslinking and crystalline domains.[36] The crystallization trend revealed by XRD was highly consistent with the evolution of ordered hydrogen-bonded carbonyls observed by FTIR. The additional PPDI hard segments introduced at higher hard segments were not randomly distributed; instead, they were driven by strong hydrogen bonding to align and pack into stable crystalline structures.[37] This synergistic interaction between hydrogen-bond-induced crystallization and microphase separa-

tion forms the structural basis for the excellent mechanical properties of this material.

Thermomechanical Properties

Fig. 5(a) proposes a molecular-level model to visually interpret the mechanism by which the hard segment content regulates the microstructural evolution, hydrogen bonding networks, and crystallization behavior. The orange segments represent soft segments, purple short chains represent hard segments, red dots denote hydrogen bonds, and circled purple area corresponds to the crystalline region. At low hard segment contents, the hard segments are sparsely dispersed with weak hydrogen bonding, forming only isolated aggregates without long-range order. As the hard segment content increased, the density of hydrogen bonds increased, driving aggregation and inducing local crystallization. At higher concentrations, the PPDI hard segments self-assembled to form a dense and interconnected physical network owing to their inherent structural symmetry and strong hydrogen bonding capabilities. These highly crystalline domains acted as a robust supporting skeleton throughout the soft matrix, marking a transition from isolated domains to a percolated network structure.[38]

This microstructural evolution governs the macroscopic thermomechanical properties. TMA analysis (Fig. 5b and Table S4 in ESI) reveals a substantial enhancement in thermal resistance, with the softening temperature at 5% strain ($T_{\varepsilon=5\%}$)

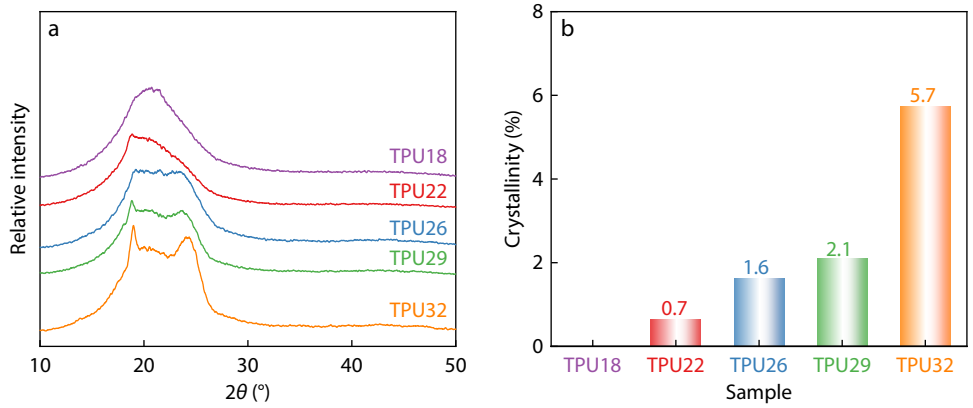

Fig. 4 (a) XRD patterns of TPUs; (b) Crystallinity histogram of different TPUs.

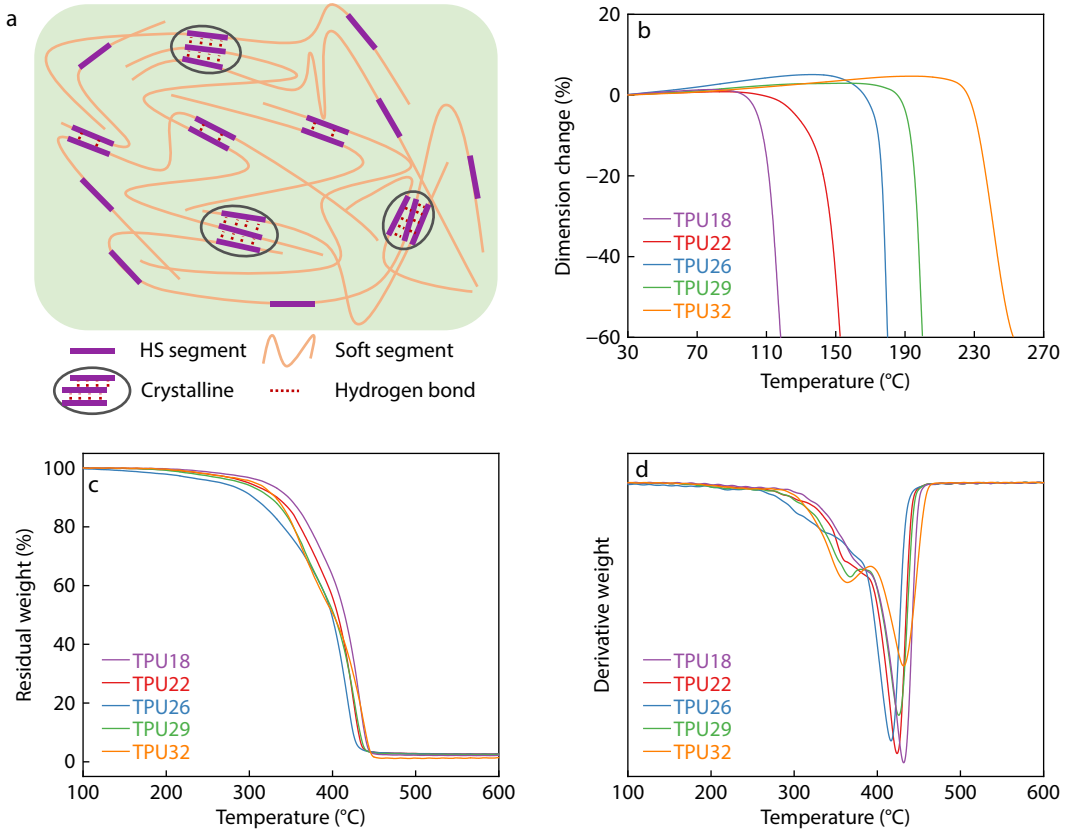

Fig. 5 (a) Schematic of the microstructural evolution mechanism; (b) TMA curves of TPUs; (c) TGA curves of TPUs; (d) DTG curves of TPUs.

https://doi.org/10.1007/s10118-026-3668-8

increasing from 104.9 °C for TPU18 to 230.2 °C for TPU32. The key mechanism behind this significant enhancement lies in the qualitative change in the physical crosslinking efficiency, where the high content of hard segments assembles into highly stable rigid crystalline regions through strong hydrogen bonding, thus constructing a robust three-dimensional network framework that acts as a thermal anchoring point.[39] A denser network requires higher energy for dissociation, thereby enabling the material to resist macroscopic deformation at elevated temperatures.

The TGA and DTG curves (Figs. 5c and 5d) reveal a typical two-stage thermal degradation behavior for all samples (data in Table S5 in ESI). The first stage corresponds to the scission of urethane bonds in the hard segments, whereas the second stage involves the degradation of polyol soft chains.[40] Notably, the decomposition temperature of the first stage shifted significantly higher with increasing hard segment content. This suggests that the highly ordered and crystalline hard domains provide a protective effect, restricting the chain mobility and delaying the onset of urethane bond dissociation. This aligns perfectly with the XRD and FTIR findings, confirming that a higher hard segment content promotes a denser hydrogen bond network and more ordered aggregation structure.

Mechanical Properties and Dynamic Thermomechanical Analysis

The static tensile behavior of the TPUs is presented in Figs. 6(a) and 6(b), with the detailed data listed in Table S6 (in ESI). The results clearly demonstrate that, at a constant soft-segment molecular weight, the hard segment content plays a decisive role in reinforcing the mechanical strength. As hard segment content increases, the tensile strength increases from 6.1 MPa to 22.6 MPa, the modulus at 100% strain rises from 1.8 MPa to 14.1 MPa, and the Shore A hardness escalates from 65 to 95. This significant reinforcement effect is attributed to the microstructural evolution: a higher hard segment content promotes the formation of highly crystalline, high-modulus hard domains *via* ordered hydrogen bonding. These domains acted as rigid physical crosslinks within the soft matrix, effectively bearing the applied load. The proliferation of rigid domains inevitably restricts the conformational freedom of the PO3G soft segments, reducing the elongation at break from 1747% to 640%. It is noteworthy that TPU32 retained an elongation exceeding 600%. This highlights the intrinsic high elasticity and flexibility of the soft segment, endowing the TPU samples with an excellent balance between high strength and deformability.

DMA further elucidated the viscoelastic behavior over a wide temperature range (Figs. 6c and 6d and Table S7 in ESI). In the glassy region, all samples exhibited similar stiffness with storage modulus (E') magnitudes of approximately 10^9 Pa. Upon heating through the glass transition into the rubbery plateau, E' drops by orders of magnitude, but the extent of this drop decreases significantly with increasing hard segment content. Specifically, at 100 °C, the E' of TPU18 decreased to 10^7 Pa, whereas TPU32 maintained a robust E' of 10^8 Pa. This indicates that the dense physical crosslinking network formed by the high hard segment content significantly enhances the cohesive force between hard segments, imparting superior high-temperature dimensional stability and creep resistance. $\tan\delta_{max}$ exhibited a clear declining trend

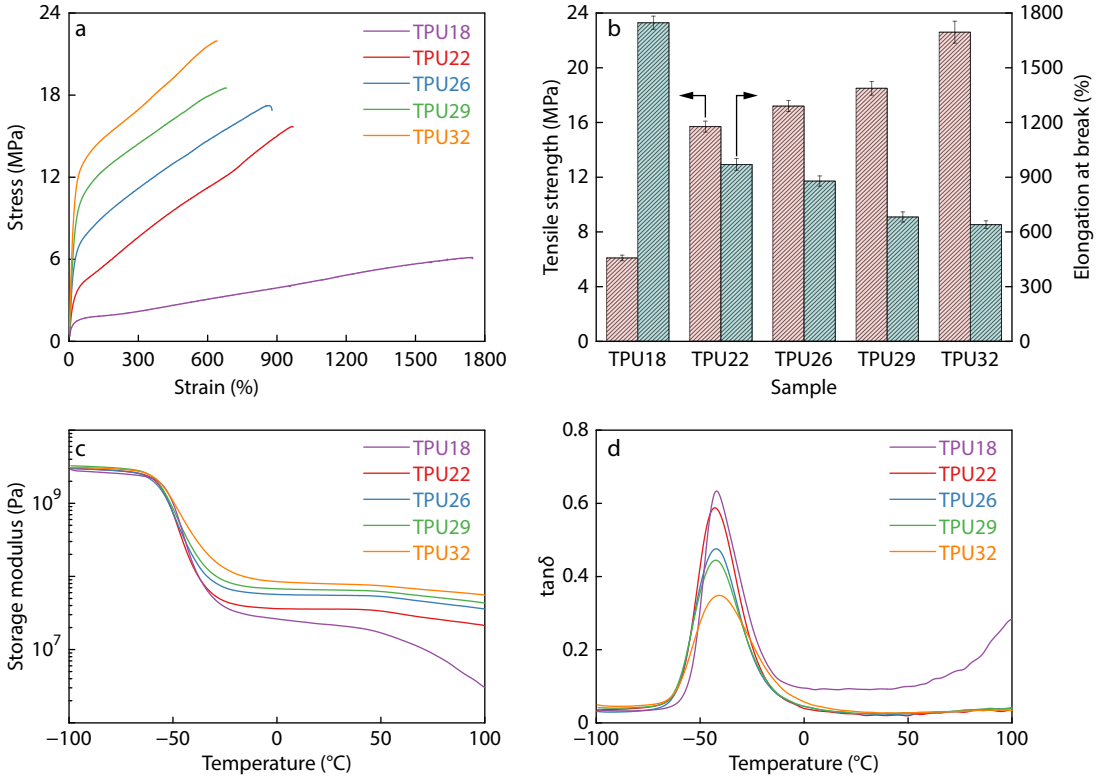

Fig. 6 (a) Stress-strain curves of TPUs; (b) Comparison of mechanical properties of TPUs; (c) Storage modulus versus temperature of TPUs; (d) tanδ versus temperature of TPUs.

(from 0.65 to 0.35) with increasing hard segment content. The dense crystalline domains at high hard segment contents impose strong constraints on the motion of the surrounding soft segments. The cooperative motion of the soft segments during relaxation was suppressed, and the energy dissipation was reduced, resulting in a lower damping peak. This result further corroborates the effective regulation of the hard segment content in the microphase-separated structure and interfacial interactions.

CONCLUSIONS

In this study, a series of bio-based TPUs based on PPDI and PO3G were successfully synthesized *via* a two-step prepolymer method. The regulatory mechanisms of the hard segment content on the microphase separation behavior, aggregation structure, and macroscopic properties were systematically elucidated. As the hard segment content increased from 18% to 32%, the high structural symmetry of the PPDI hard segments facilitated the construction of a hydrogen-bonding network (the fraction of hydrogen-bonded carbonyls increased significantly from 59.1% to 85.8%) and refinement of the crystallization behavior (crystallinity increased from 0.7% to 5.7%). These enhanced physical interactions exacerbated the thermodynamic incompatibility between segments, leading to an increase in the microphase separation long period from 14.2 nm to 15.2 nm. Moreover, the high hard segment content significantly strengthened the rigidity and stability of the physically crosslinked network. Consequently, TPU32 exhibited a tensile strength of 22.6 MPa, a Shore A hardness of 95, and an excellent $T_{\varepsilon=5\%}$ of 230.2 °C, representing a substantial improvement over the low hard segment content TPU18 ($T_{\varepsilon=5\%}$=104.9 °C). This demonstrates that by controlling the hard segment content, the material properties can be precisely tailored across a wide range, from excellent elasticity to high strength and heat resistance. These findings provide a critical structural regulation blueprint for the rational design of novel elastomers that integrate superior mechanical strength, thermal resistance, and ecological sustainability.

Conflict of Interests

The authors declare no interest conflict.

Electronic Supplementary Information

Electronic supplementary information (ESI) is available free of charge in the online version of this article at http://doi.org/10.1007/s10118-026-3668-8.

Data Availability Statement

The data that support the findings of this study are available from the corresponding author upon reasonable request.

ACKNOWLEDGMENTS

This work was financially supported by the National Key Research and Development Program of China (No. 2024YFB3713000) and the National Natural Science Foundation of China (Nos. 52203003 and 52250357).

REFERENCES

1 Balko, J.; Fernández-d'Arlas, B.; Pöselt, E.; Dabbous, R.; Müller, A. J.; Thurn-Albrecht, T. Clarifying the origin of multiple melting of segmented thermoplastic polyurethanes by fast scanning calorimetry. *Macromolecules* **2017**, *50*, 7672–7680.
2 Fei, Z. X.; Yin, C.; Sun, J. R.; Yuan, L.; Shi, L. Y. Healable and recyclable multiblock polyurethanes with mechanical performance tailorability based on hierarchical phase separation and dynamic bond interaction. *Polymer* **2023**, *289*, 126467.
3 Backes, E. H.; Harb, S. V.; Pinto, L. A.; de Moura, N. K.; de Morgado, G. F. M.; Marini, J.; Pessan, L. A. Thermoplastic polyurethanes: synthesis, fabrication techniques, blends, composites, and applications. *J. Mater. Sci.* **2024**, *59*, 1123–1152.
4 Duval, A.; Sarbu, A.; Dalmas, F.; Albertini, D.; Avérous, L. 2,3-butanediol as a biobased chain extender for thermoplastic polyurethanes: influence of stereochemistry on macromolecular architectures and properties. *Macromolecules* **2022**, *55*, 5371–5381.
5 Rajput, B. S.; Forman, A.; Halloran, M. W.; Hai, T. A. P.; Scofield, G. B.; Burkart, M. D. Variation of aliphatic diisocyanates in bio-based TPUs. *Macromolecules* **2023**, *56*, 8813–8822.
6 Xie, D. M.; Zhang, Y. X.; Li, Y. D.; Weng, Y.; Zeng, J. B. Castor oil-derived sustainable poly(urethane urea) covalent adaptable networks with tunable mechanical properties and multiple recyclability based on reversible piperidine-urea bond. *Chem. Eng. J.* **2022**, *446*, 137071.
7 Mei, X.; Lu, W.; Dong, J. R.; Pan, K. H.; Tan, J. J.; Yan, H. Y.; Chen, H. X. Influence of soft segment length on the dielectric polarization behavior of ketal-containing polyurethane elastomer. *Chinese J. Polym. Sci.* **2025**, *44*, 189–197.
8 He, Y.; Xie, D.; Zhang, X. The structure, microphase-separated morphology, and property of polyurethanes and polyureas. *J. Mater. Sci.* **2014**, *49*, 7339–7352.
9 Qiu, J.; Zhao, H.; Luan, S.; Wang, L.; Shi, H. Recent advances in functional polyurethane elastomers: from structural design to biomedical applications. *Biomater. Sci.* **2025**, *13*, 2526–2540.
10 Li, K.; Yan, X.; Wang, Y.; Ai, T.; Niu, Y.; Chen, Y. Design and modification mechanism of a novel high-viscosity thermoplastic polyurethane modified asphalt. *Constr. Build. Mater.* **2024**, *433*, 136585.
11 Zeng, Y.; Chen, Y.; Sha, D.; Wu, Y.; Qiu, R.; Liu, W. Highly stretchable fatty acid chain-dangled thermoplastic polyurethane elastomers enabled by H-bonds and molecular chain entanglements. *ACS Sustainable Chem. Eng.* **2022**, *10*, 11524–11532.
12 Xu, W.; Zhang, R.; Liu, W.; Zhu, J.; Dong, X.; Guo, H.; Hu, G. H. A multiscale investigation on the mechanism of shape recovery for IPDI to PPDI hard segment substitution in polyurethane. *Macromolecules* **2016**, *49*, 5931–5944.
13 Wu, Y.; Xu, C.; Gan, M.; Zhai, M.; Chen, Z.; Shou, T.; Hu, G. H. Multifunctional bio-based waterborne polyurethane with excellent transparency, strength, abrasion resistance, and antimicrobial properties. *Prog. Org. Coat.* **2024**, *195*, 108671.
14 Jia, Y.; Guan, Q.; Chu, C.; Zhang, L.; Neisiany, R. E.; Gu, S.; You, Z. A fluorine-based strong and healable elastomer with unprecedented puncture resistance for high performance flexible electronics. *Sci. Bull.* **2024**, *69*, 1875–1886.
15 Shen, A.; Xuan, H.; Jia, Y.; Gu, S.; Neisiany, R. E.; Shu, W.; You, Z. Dynamic healing-assembly for biocompatible, biodegradable,

Graphical Abstract

Regulation of Microphase Separation in Bio-based Thermoplastic Polyurethanes Driven by Hard Segment Content

De-Xian Yin, Yu-Qiong Hu, Ya-Nan Cheng, Shuo Yan, Zi-Lin Liu, Yi-Qing Wang, Shi-Kai Hu, and Xiu-Ying Zhao

Beijing University of Chemical Technology

Regulating hard segment content in bio-based 1,4-phenylene diisocyanate (PPDI) polyurethanes optimizes microphase separation and induces ordered crystallization. This significantly enhances the 5% thermal deformation temperature to 230.2 °C and tensile strength to 22.6 MPa, providing a robust strategy for sustainable, high-performance elastomers.

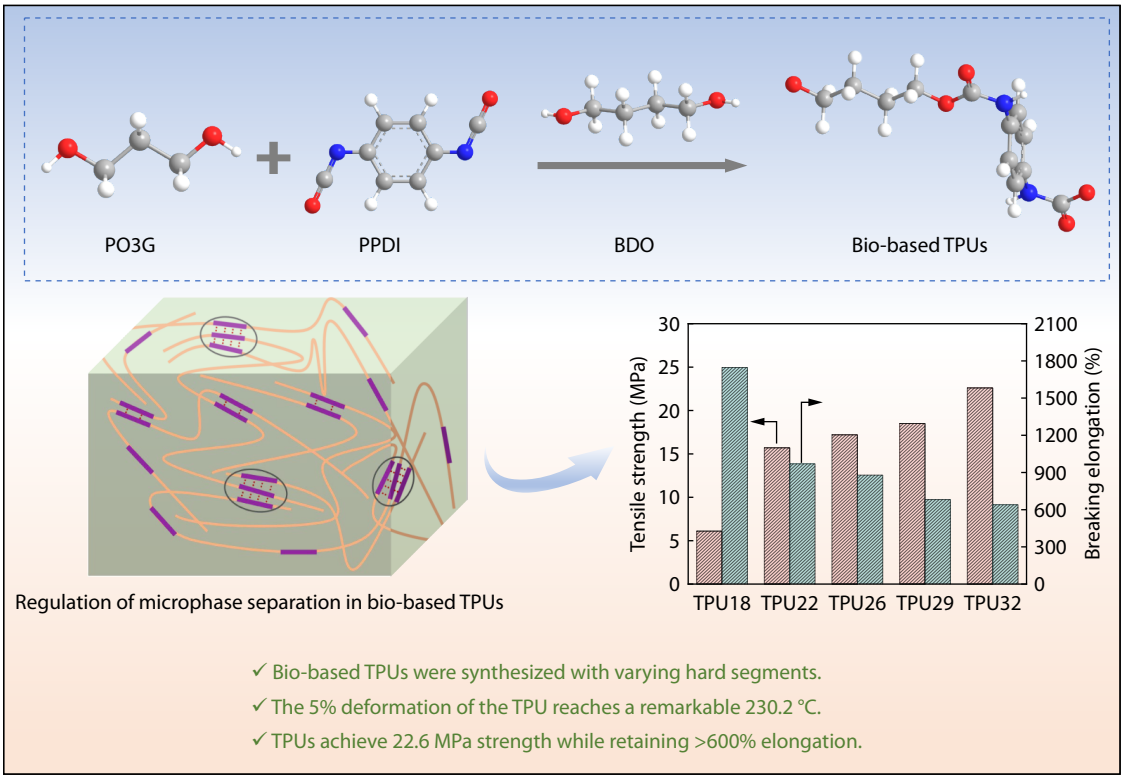

Chinese J. Polym. Sci. 2026, 44, 2748–2757 *https://doi.org/10.1007/s10118-026-3668-8*

stretchable and self-healing triboelectric nanogenerators. *Chem. Eng. J.* **2024**, *491*, 151896.
16 Zhang, W.; Xuan, H.; Xu, X.; Lou, J.; Guan, Q.; You, Z. Multiple dynamic bonds enable high mechanical strength and efficient room-temperature self-healable polyurethane for triboelectric nanogenerators. *Sci. China Chem.* **2025**, *68*, 1468–1477.
17 Jia, Y.; Chu, C.; Wu, Z.; Ni, Y.; Cao, S.; Liao, T.; You, Z. Simultaneous improvement of mechanical strength, toughness, and self-healability of elastomers enabled by F—H-bond-based nanoconfinement. *Angew. Chem. Int. Ed.* **2025**, *64*, e202505848.
18 Jia, Y.; Chu, C.; Cao, S.; Wu, Z.; Gu, S.; Chen, Z.; You, Z. Self-confined effects induced by F—H bonds simultaneously enhance mechanical strength, conductivity, and self-healability of ionic elastomers. *Adv. Funct. Mater.* **2025**, *36*, e26628.
19 Gaymans, R. J. Segmented copolymers with monodisperse crystallizable hard segments: Novel semi-crystalline materials. *Prog. Polym. Sci.* **2011**, *36*, 713–748.
20 Amirkhosravi, M.; Yue, L.; Ju, T.; Manas-Zloczower, I. Designing thermal annealing to control mechanical performance of thermoplastic polyurethane elastomers. *Polymer* **2021**, *214*, 123254.
21 Yang, J. X.; Qian, H. J.; Gong, Z.; Lu, Z. Y.; Cui, S. X. Stretching elasticity and flexibility of single polyformaldehyde chain. *Chinese J. Polym. Sci.* **2022**, *40*, 333–337.
22 Pérez-Camargo, R. A.; Meabe, L.; Liu, G.; Sardon, H.; Zhao, Y.; Wang, D.; Müller, A. J. Even–odd effect in aliphatic polycarbonates with different chain lengths: From poly (hexamethylene carbonate) to poly (dodecamethylene carbonate). *Macromolecules* **2020**, *54*, 259–271.
23 Zhang, L.; Huang, H.; Sun, L.; Ma, X.; Tan, H.; You, Z. Sequence-controlled dynamic covalent units enable decoupling of mechanical and self-healing performance of polymers. *Sci. China*

Chem. **2024**, *68*, 745–753.
24 Cheng, B. X.; Gao, W. C.; Ren, X. M.; Ouyang, X. Y.; Zhao, Y.; Zhao, H.; Li, R. K. A review of microphase separation of polyurethane: Characterization and applications. *Polym. Test.* **2022**, *107*, 107489.
25 Gao, X.; Qian, H.; Wang, J.; Hong, Y.; Chen, Y.; Zhao, L.; Hu, D. Self-reinforced thermoplastic polyurethane composite with excellent mechanical properties, heat resistance and sustainable recycling. *Compos. Part B Eng.* **2025**, *297*, 112342.
26 Farid, M. I.; Wu, W.; Li, G.; Zheng, A.; Zhao, Y. Superior tensile properties of FDM 3D-printed TPU/E-TPU layered structure. *J. Mater. Res.* **2024**, *39*, 2051–2066.
27 Ti, Y.; Chen, D. Temperature dependence of hydrogen bond in fe-OCAP/polyurethane blends. *J. Appl. Polym. Sci.* **2013**, *130*, 2265–2271.
28 Sofla, R. L. M.; Rezaei, M.; Babaie, A.; Nasiri, M. Preparation of electroactive shape memory polyurethane/graphene nanocomposites and investigation of relationship between rheology, morphology and electrical properties. *Compos. Part B Eng.* **2019**, *175*, 107090.
29 Chen, Z.; Wang, J.; Zhao, W.; Hu, S.; Yin, D.; Zhao, X. Synergistic dual-crosslinking and multilevel hydrogen-bond engineering for high-damping polyurethanes. *Constr. Build. Mater.* **2026**, *514*, 145569.
30 Yin, D.; Liu, Y.; Wang, X.; Hu, S.; Liu, L.; Zhao, X.; Zhang, L. Novel bio-based polyurethane elastomers for adjustable room-temperature damping property. *Compos. Commun.* **2024**, *49*, 101975.
31 Ning, N.; Qin, H.; Wang, M.; Sun, H.; Tian, M.; Zhang, L. Improved dielectric and actuated performance of thermoplastic polyurethane by blending with XNBR as macromolecular dielectrics. *Polymer* **2019**, *179*, 121646.
32 Wang, X.; Yin, D.; Chen, Z.; Hu, Y.; Hu, S.; Zhao, X. CO_2-based polyurethane elastomers with enhanced mechanical and tunable room-temperature damping performances. *Eur. Polym. J.* **2024**, *220*, 113499.
33 Wang, H.; Li, Y.; Zhang, H.; Lang, X.; Wang, X.; Cao, L.; Zong, C. Effects of soft segment molecular weight on the properties of recyclable polyurethanes with low-temperature multiple shape memory. *J. Polym. Sci.* **2024**, *63*, 121–132.
34 Gong, X.; Liu, Q.; Chen, P.; Wang, H.; Liu, X.; Chen, S.; Wu, S. Modification mechanism of green polyurethane modified asphalt prepared by in-situ polymerization. *Constr. Build. Mater.* **2024**, *448*, 138243.
35 Fernández-d'Arlas, B.; Ugarte, L.; Eceiza, A.; Müller, A. J. Chemical composition and mechanical deformation define lamellar sizes in aliphatic triblock-based polyurethane elastomers. *Macromolecules* **2024**, *57*, 7755–7767.
36 Huang, M.; Li, Z.; Xu, W.; He, S.; Liu, W.; Jiang, L.; Liu, H. Visualization and quantification of microphase separation in thermoplastic polyurethanes under different hard segment contents and its effect on the mechanical properties. *Polym. Test.* **2024**, *131*, 108329.
37 Amjed, N.; Bhatti, I. A.; Simon, L.; Castel, C. D.; Zia, K. M.; Zuber, M.; Murtaza, M. A. Preparation and characterization of thermoplastic polyurethanes blended with chitosan and starch processed through extrusion. *Int. J. Biol. Macromol.* **2022**, *208*, 37–44.
38 Xiao, Y.; Jiang, L.; Liu, Z.; Yuan, Y.; Yan, P.; Zhou, C.; Lei, J. Effect of phase separation on the crystallization of soft segments of green waterborne polyurethanes. *Polym. Test.* **2017**, *60*, 160–165.
39 Hu, S.; He, S.; Wang, Y.; Wu, Y.; Shou, T.; Yin, D.; Zhang, L. Self-repairable, recyclable and heat-resistant polyurethane for high-performance automobile tires. *Nano Energy* **2022**, *95*, 107012.
40 Lukoschek, S.; Frankenbach, L. A.; Kruppke, I.; Cherif, C. Biobased TPU for melt spun multifilament yarns as a sustainable alternative for conventional fossil based TPU. *J. Polym. Environ.* **2025**, *33*, 1934–1946.

https://doi.org/10.1007/s10118-026-3668-8